Modeling Sorbent Injection for Mercury Control in Baghouse Filters: I—Model Development and Sensitivity Analysis

Joseph R.V. Flora
Department of Civil and Environmental Engineering, University of South Carolina, Columbia, South Carolina

Richard A. Hargis, William J. O'Dowd, and Henry W. Pennline
National Energy Technology Laboratory, U.S. Department of Energy, Pittsburgh, Pennsylvania

Radisav D. Vidic
Department of Civil and Environmental Engineering, University of Pittsburgh, Pittsburgh, Pennsylvania

ABSTRACT

A two-stage mathematical model for Hg removal using powdered activated carbon injection upstream of a baghouse filter was developed, with the first stage accounting for removal in the ductwork and the second stage accounting for additional removal caused by the retention of carbon particles on the filter. The model shows that removal in the ductwork is minimal, and the additional carbon detention time from the entrapment of the carbon particles in the fabric filter enhances the Hg removal from the gas phase. A sensitivity analysis on the model shows that Hg removal is dependent on the isotherm parameters, the carbon pore radius and tortuosity, the C/Hg ratio, and the carbon particle radius.

INTRODUCTION

Mercury control models represent a combination of the microscale models that account for the kinetics of the adsorption process on the adsorbent particle and the macroscale processes that account for the mass balance in the reactor system used to control gaseous emissions. Microscale models typically include the external (film) resistance to transport and internal transport inside the sorbent particle. External resistance to transport is usually modeled according to Fick's first law of diffusion, while intraparticle transport can be broadly classified in the following categories: (1) pore diffusion, (2) surface diffusion, and (3) dual pore and surface diffusion.

Chen and co-workers[1,2] developed one of the first and simplest Hg control models. Their model describes Hg removal by powdered sorbent injected into the flue gas duct but does not account for the impact of particulate control devices used later in the process (i.e., electrostatic precipitator or fabric filter). The authors assumed that all Hg molecules that diffuse across the external film are completely captured by the sorbent particle. External resistance to mass transfer was modeled by Fick's first law assuming negligible concentration of Hg on the external surface of the adsorbent particle. These authors also offered a simplified solution to the transport equation inside the sorbent particle (assuming the small uptake of adsorbate relative to the total amount of adsorbate in the batch reactor).

Flora et al.[3] developed a model for a closed-batch reactor system that accounted for both external mass transfer resistance and intraparticle transport. External mass transfer was modeled using Fick's first law, while the intraparticle transport was modeled using the surface diffusion transport mechanism. They used the model to estimate equilibrium (Langmuir isotherm) and kinetic parameters (D_s and k_f) from closed-batch Hg uptake experiments, and developed simple design nomograms for 80 and 90% Hg removal in the duct. One of the major drawbacks of this study is that the kinetic and adsorption

IMPLICATIONS

The mathematical model developed in this study offers significant benefits in estimating appropriate design and operating strategies that would lead to efficient and economic control of Hg emissions from coal-fired power plants and utility boilers. This model incorporates key mass transfer and equilibrium processes that govern adsorption of Hg vapors on activated carbon in the duct and on the fabric filter. Sensitivity analyses suggested that the key parameters that have a major impact on Hg removal efficiency include the C/Hg ratio and the carbon particle size.

parameters were obtained from experimental data that were collected using pure N_2 as a carrier gas. Thus, the parameters of their model do not account for the effect of other chemical reactions that may be catalyzed by the carbon surface in the presence of reactive gases that are typical for coal-fired power plants. In addition, the experimental data were obtained using unreasonably high Hg concentrations because of the inherent limitations of the analytical procedures used to measure Hg concentrations in the gas phase.

Meserole et al.[4] extended the model of Chen and co-workers[1,2] to account for the additional Hg removal that is encountered as a result of the extended contact time between the sorbent particle and Hg on the fabric filter. Mercury removal in the duct was assumed to be external mass transfer-limited and the model did not incorporate any terms to account for intraparticle diffusion. Additional Hg removal on the fabric filter was modeled using the fixed-bed reactor model coupled with an external mass transfer limited diffusion model. Adsorption equilibrium parameters for the Freundlich isotherm were obtained by fitting the model to breakthrough curves obtained from fixed-bed laboratory-scale experiments with simulated flue gas. These parameters were subsequently used to assess Hg removal in the duct and evaluate the impact of Hg concentration and particle size on the removal efficiency. Mercury removal on the fabric filter was modeled using the prediction from a fixed-bed reactor model that assumed a bed thickness corresponding to a 45-min accumulation time and complete cleaning of the fabric filter after that period.

Serre et al.[5] used the same external mass transfer model as Chen and co-workers[1,2] to assess the largest sorbent particle size that would reduce the effect of external mass transfer resistance on Hg uptake in the entrained-flow reactor. They suggested that a particle size of 14 μm or less would be sufficient to minimize external mass transfer effects.

Serre and Silcox[6] developed a model for a baghouse describing Hg removal in fly ash injected for Hg control. They accounted for Hg removal in the ductwork and in the baghouse. To our knowledge, this was the first model to address the moving boundary problem associated with a growing adsorbent layer on a filter bed. More recently, Scala[7,8] also developed a model describing Hg removal via carbon adsorption in the duct and on the carbon entrained in a fabric filter. Because the model developed by Scala[7,8] is similar to the model developed in this study, a comparison of the model presented in this paper and the published model is discussed at the end of the Results and Discussion section to facilitate understanding of the differences between the two models.

The objective of this study was to develop a model that describes Hg removal using activated carbon in a baghouse filter. In the first paper of this series, the model development and solution procedure are described in detail and a sensitivity analysis is performed to evaluate the parameters that impact the calculated Hg removal from the system. In Part II of this article, model parameters are estimated using a subset of the data collected from a pilot-scale system and the model predictions are verified using the rest of the data from the same system.

MATHEMATICAL MODEL

A two-stage model describing Hg removal from the gas phase by activated carbon injection and subsequent deposition and removal in a baghouse filter is developed using the pore diffusion model (PDM) to describe the kinetics of adsorption of Hg from the carbon surface into the activated carbon particle. The first stage involves coupling the PDM to a model for a plug flow system to describe Hg uptake in the ductwork, while the second stage involves coupling the PDM to a model for a packed bed. In the second stage, the growth and deposition of the activated carbon particles on the baghouse filter is incorporated in the model to account for additional Hg uptake of the particles because of an increased detention time in the system. The key assumptions for the model are

(1) Removal of Hg from the bulk is caused solely by adsorption on the activated carbon;
(2) The activated carbon particle is isothermal, and the adsorption equilibrium between the activated carbon pores and the gas phase is described by the Langmuir isotherm;
(3) The activated carbon particles are all spherical, uniform in size, uniformly dispersed in the gas phase, and uniformly distributed within the packed bed;
(4) A mass transfer boundary layer causes resistance to mass transfer from the bulk to the activated carbon surface, and mass transfer within the activated carbon particle is controlled by pore diffusion; and
(5) As a first approximation, the flow rate across the baghouse filter cake is assumed to be constant with time. It is recognized that the pressure buildup across the baghouse filter with the accumulation of fly ash will result in a flow rate decrease with time.

Characterization of the forward and backward rates of adsorption on the surface of an adsorbent is difficult when there is intraparticle diffusional resistance to mass transfer. Thus, the approach taken in this study to model for the time-dependent adsorption process was to account for mass transfer resistance coupled with

adsorption equilibrium because the adsorption process is usually not the rate-limiting step.[9]

First Stage

A mass balance on Hg in the activated carbon particle and the bulk can be written as

$$\rho_p(1-\varepsilon_p)\frac{\partial q_p}{\partial t}+\varepsilon_p\frac{\partial c_p}{\partial t}=\varepsilon_p\frac{D_p}{r^2}\frac{\partial}{\partial r}r^2\frac{\partial c_p}{\partial r} \tag{1}$$

$$Q\frac{dc_b}{dt}=-\dot{m}_c\left(\frac{dq_{ave,p}}{dt}+\frac{\varepsilon_p}{\rho_p(1-\varepsilon_p)}\frac{dc_{ave,p}}{dt}\right) \tag{2}$$

where

$$q_{ave,p}=\frac{3}{r_p^3}\int_0^{r_p}q_p(r,t)r^2dr \tag{3}$$

$$c_{ave,p}=\frac{3}{r_p^3}\int_0^{r_p}c_p(r,t)r^2dr \tag{4}$$

$$q_p(r,t)=\frac{q_{max}bc_p(r,t)}{1+bc_p(r,t)} \tag{5}$$

Equations 1 and 2 are subject to the following initial and boundary conditions:

$$c_p(r,t=0)=0 \tag{6}$$

$$c_b(t=0)=c_o \tag{7}$$

$$\frac{\partial c_p(r=0,t)}{\partial r}=0 \tag{8}$$

$$\varepsilon_p D_p\frac{\partial c_p(r=r_p,t)}{\partial r}=k_f[c_b-c_p(r=r_p,t)] \tag{9}$$

Using the following dimensionless variables

$$C_p=\frac{c_p}{c_o};\ Q_p=\frac{q_p}{q_o};\ T_d=\frac{D_p t}{r_p^2};\ R=\frac{r}{r_p};\ Bi_d=\frac{k_f r_p}{\varepsilon_p D_p}$$
$$\lambda_1=\frac{q_o\rho_p(1-\varepsilon_p)}{c_o\varepsilon_p};\ \lambda_2=\frac{\dot{m}_c q_o}{Qc_o};\ \lambda_3=\frac{\lambda_2}{\lambda_1}=\frac{\dot{m}_c\varepsilon_p}{Q\rho_p(1-\varepsilon_p)} \tag{10}$$

where

$$q_o=\frac{q_{max}bc_o}{1+bc_o} \tag{11}$$

Equations 1–9 can be rewritten in the following dimensionless format:

$$\lambda_1\frac{\partial Q_p}{\partial T_d}+\frac{\partial C_p}{\partial T_d}=\frac{1}{R^2}\frac{\partial}{\partial R}R^2\frac{\partial C_p}{\partial R} \tag{12}$$

$$\frac{dC_b}{dT_d}=-\lambda_2\frac{dQ_{ave,p}}{dT_d}-\lambda_3\frac{dC_{ave,p}}{dT_d} \tag{13}$$

$$Q_{ave,p}=3\int_0^1 Q_p(R,T)R^2dR \tag{14}$$

$$C_{ave,p}=3\int_0^1 C_p(R,T)R^2dR \tag{15}$$

$$Q_p(R,T)=C_p(R,T)\frac{1+bc_o}{1+C_p(R,T)\times bc_o} \tag{16}$$

$$C_p(R,T_d=0)=0 \tag{17}$$

$$C_b(T_d=0)=1 \tag{18}$$

$$\frac{\partial C_p(R=0,T_d)}{\partial R}=0 \tag{19}$$

$$\frac{\partial C_p(R=1,T_d)}{\partial R}=Bi_d[C_b-C_p(R=1,T_d)] \tag{20}$$

Second Stage

Figure 1 shows the coordinate system used to describe the packed bed. A mass balance on Hg in a packed bed can be written as

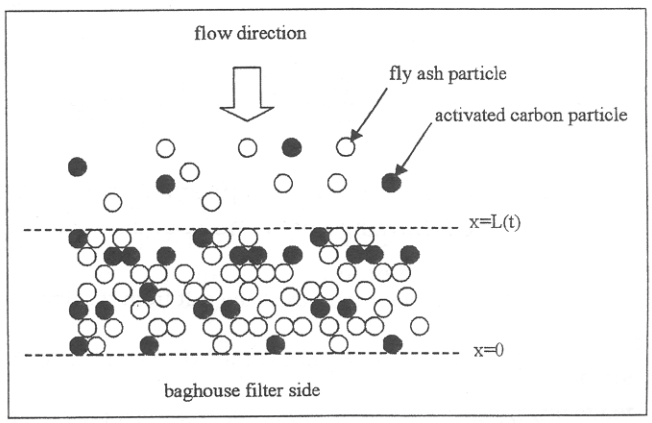

Figure 1. A growing bed.

$$\varepsilon_b \frac{\partial c_b}{\partial t} + \varepsilon_{cb}\left(\rho_p(1-\varepsilon_p)\frac{\partial q_{ave,p}}{\partial t} + \varepsilon_p \frac{\partial c_{ave,p}}{\partial t}\right) = \varepsilon_b v \frac{\partial c_b}{\partial x} + \varepsilon_b D \frac{\partial^2 c_b}{\partial x^2} \tag{21}$$

subject to the following initial and boundary conditions:

$$q(r, t = 0) = \text{conditions at the exit from the first stage} \tag{22}$$

$$c_p(r, t = 0) = \text{conditions at the exit from the first stage} \tag{23}$$

$$c_b(x, t = 0) = \text{bulk conditions at the exit from the first stage} \tag{24}$$

$$\frac{\partial c_b(x = 0, t)}{\partial x} = 0 \tag{25}$$

$$\int_0^{L(t)} \left[\varepsilon_b \frac{\partial c_b}{\partial t} + \varepsilon_{cb}\left(\rho_p(1-\varepsilon_p)\frac{\partial q_{ave,p}}{\partial t} + \varepsilon_p \frac{\partial c_{ave,p}}{\partial t}\right)\right] A dx = Q[c_b(x = L(t), t) - c_b(x = 0, t)] \tag{26}$$

Using a mass balance expression (eq 26) in lieu of specifying the bulk concentration at the top of the packed bed [$x = L(t)$] to be equal to the influent concentration results in a concentration discontinuity at the boundary but guarantees mass balance closure across the packed bed. The growth of the packed bed with time is described by

$$L(t) = L_o + \frac{\dot{m}_c}{\rho_p(1-\varepsilon_p)\varepsilon_{cb}A} t \tag{27}$$

Equations 21–27 in conjunction with eq 1 describe the mass balance on Hg for a carbon particle within the packed bed. The boundary conditions for eq 1 and eqs 8 and 9.

Equations 21 and 1 can be rewritten in the following dimensionless format:

$$\frac{\partial C_b}{\partial T_f} + E\left(\lambda_1 \frac{\partial Q_{ave,p}}{\partial T_f} + \frac{\partial C_{ave,p}}{\partial T_f}\right) = \frac{\partial C_b}{\partial X} + \frac{1}{Pe}\frac{\partial^2 C_b}{\partial X^2} \tag{28}$$

$$\lambda_1 \frac{\partial Q_p}{\partial T_f} + \frac{\partial C_p}{\partial T_f} = \lambda_4 \frac{1}{R^2}\frac{\partial}{\partial R} R^2 \frac{\partial C_p}{\partial R} \tag{29}$$

with equivalent eqs 14–16, 19, and 20 still applicable and with the following initial and boundary conditions:

$$Q_p(R, T_f = 0) = \text{conditions at the exit from the first stage} \tag{30}$$

$$C_p(R, T_f = 0) = \text{conditions at the exit from the first stage} \tag{31}$$

$$C_b(X, T_f = 0) = \text{bulk conditions at the exit from the first stage} \tag{32}$$

$$\frac{\partial C_b(X = 0, T_f)}{\partial X} = 0 \tag{33}$$

$$\int_0^{X(T_f)} \left[\frac{\partial C_b}{\partial T_f} + E\left(\lambda_1 \frac{\partial Q_{ave,p}}{\partial T_f} + \frac{\partial C_{ave,p}}{\partial T_f}\right)\right] dX = C_b(X = X(T_f), T_f) - C_b(X = 0, T_f) \tag{34}$$

$$X(T_f) = X_o + B_g T_f \tag{35}$$

where

$$X = \frac{x}{L_{max}};\ T_f = \frac{tv}{L_{max}};\ Pe = \frac{vL_{max}}{D}$$
$$E = \frac{\varepsilon_{cb}\varepsilon_p}{\varepsilon_b};\ \lambda_4 = \frac{D_p L_{max}}{r_p^2 v};\ B_g = \frac{\dot{m}}{\rho_p(1-\varepsilon_p)\varepsilon_{cb}Av} \tag{36}$$

Model Solution

For the first stage, eq 12 was reduced to ordinary differential equations using orthogonal collocation methods[10] with five-interior collocation points in the activated carbon particle. The resulting system of equations was solved using DDASSL,[11] a subroutine capable of solving algebraic and ordinary differential equations simultaneously.

For the second stage, the length of the packed bed varies with time as described by eq 35. To account for this moving boundary, the following coordinate transformation was used:[12]

$$\eta = \frac{X}{X(T_f)};\ \tau = T_f;\ \xi = R \tag{37}$$

Substituting eq 37 in the model for the second stage and applying the chain rule, the dimensionless mass balance on the column and particle can be written as

$$\frac{\partial C_b}{\partial \tau} + E\left[\lambda_1\left(\frac{\partial Q_{ave,p}}{\partial \tau} - \frac{\eta B_g}{X_0 + B_g\tau}\frac{\partial Q_{ave,p}}{\partial \eta}\right) + \frac{\partial C_{ave,p}}{\partial \tau} - \frac{\eta B_g}{X_0 + B_g\tau}\frac{\partial C_{ave,p}}{\partial \eta}\right] = \frac{1 + \eta B_g}{X_0 + B_g\tau}\frac{\partial C_b}{\partial \eta} + \frac{1}{Pe}\left(\frac{1}{X_0 + B_g\tau}\right)^2 \frac{\partial^2 C_b}{\partial \eta^2} \tag{38}$$

$$\lambda_1\left(\frac{\partial Q_p}{\partial \tau} - \frac{\eta B_g}{X_0 + B_g\tau}\frac{\partial Q_p}{\partial \eta}\right) + \frac{\partial C_p}{\partial \tau} - \frac{\eta B_g}{X_0 + B_g\tau}\frac{\partial C_p}{\partial \eta} = \lambda_4 \frac{1}{\xi^2}\frac{\partial}{\partial \xi}\xi^2 \frac{\partial C_p}{\partial \xi} \tag{39}$$

with the following initial and boundary conditions:

$$Q_p(\xi, \eta, \tau = 0) = \text{conditions at the exit from the first stage} \tag{40}$$

$C_p(\xi, \eta, \tau = 0)$ = conditions at the exit from the first stage (41)

$Q_p(\xi, \eta = 1, \tau)$ = conditions at the exit from the first stage (42)

$C_p(\xi, \eta = 1, \tau)$ = conditions at the exit from the first stage (43)

$C_b(\eta, \tau = 0)$ = bulk conditions at the exit from the first stage (44)

$$\frac{\partial C_p(\xi = 0, \eta, \tau)}{\partial \xi} = 0 \tag{45}$$

$$\frac{\partial C_p(\xi = 1, \eta, \tau > 0)}{\partial \xi} = Bi_f[C_b - C_p(\xi = 1, \eta, \tau)] \tag{46}$$

$$\frac{\partial C_b(\eta = 0, \tau)}{\partial \eta} = 0 \tag{47}$$

$$\int_0^1 \left[\frac{\partial C_b}{\partial \tau} - \frac{\eta B_g}{X_0 + B_g\tau} \frac{\partial C_b}{\partial \eta} + E\left(\lambda_1 \left(\frac{\partial Q_{ave,p}}{\partial \tau} - \frac{\eta B_g}{X_0 + B_g\tau} \frac{\partial Q_{ave,p}}{\partial \eta} \right) \right.\right.$$

$$\left.\left. + \frac{\partial C_{ave,p}}{\partial \tau} - \frac{\eta B_g}{X_0 + B_g\tau} \frac{\partial C_{ave,p}}{\partial \eta} \right) \right] (X_0 + B_g\tau) d\eta \tag{48}$$

$$= C_b(\eta = 1, \tau) - C_b(\eta = 0, \tau)$$

where

$$Q_{ave,p} = 3 \int_0^1 Q_p(\xi, \tau) \xi^2 d\xi \tag{49}$$

$$C_{ave,p} = 3 \int_0^1 C_p(\xi, \tau) \xi^2 d\xi \tag{50}$$

$$Q_p(\xi, \eta, \tau) = C_p(\xi, \eta, \tau) \frac{1 + bc_o}{1 + C_p(\xi, \tau) \times bc_o} \tag{51}$$

Equations 38–51 represent the final model for the second stage. Equations 38, 39, and 48 were reduced to ordinary differential equations using orthogonal collocation methods[10] with five interior collocation points in the activated carbon particle and seven interior collocation points in the packed bed. The resulting system of equations was solved using DDASSL.[11]

Parameter Estimation

The following equation was used to calculate the pore diffusion coefficient:[13]

$$D_p = \frac{1}{\tau_p} \left(\frac{1}{D_{Hg}} + \frac{1}{D_{Kn}} \right)^{-1} \tag{52}$$

where the diffusivity of Hg in the gas phase was estimated from the Chapman-Enskog theory,[14] and Knudsen diffusion coefficient was calculated using[15]

$$D_{Kn} = 9700 \frac{d_{pore}}{2} \left(\frac{T_k}{MW_{Hg}} \right)^{1/2} \tag{53}$$

The mass transfer coefficient in the duct was estimated using the following empirical correlation for forced convection around a solid sphere:[14]

$$\frac{2k_f r_p}{D_{Hg}} = 2.0 + 0.6 \left(\frac{2r_p v_o}{\nu} \right)^{1/2} \left(\frac{\nu}{D_{Hg}} \right)^{1/3} \tag{54}$$

The relative velocity (v_o) between the activated carbon particles and the gas stream was estimated using Stoke's Law with Cunningham's correction.[16]

The mass transfer coefficient in the baghouse filter was estimated using the following empirical correlation for a packed bed:[17]

$$\frac{2k_f r_p}{D_{Hg}} = 2.0 + 1.1 \left(\frac{2r_p v \varepsilon_b}{\nu} \right)^{0.6} \left(\frac{\nu}{D_{Hg}} \right)^{1/3} \tag{55}$$

Equation 55 intrinsically accounts for the effects of dispersion in the packed bed, which is calculated from[17]

$$D = \frac{20}{\varepsilon_b} D_{Hg} + v r_p \tag{56}$$

Physical characteristics of Norit Darco FGD carbon were used in the parameterization of the model. The median pore diameter was reported to be 150 Å[18] and was used in estimating D_{Kn}. The activated carbon density (ρ_p = 2.04 g/cm^3) and porosity (ε_p = 0.67) were provided by the manufacturer. Yang[19] reports that the tortuosity (τ_p) for activated carbons ranges from 5 to 65, and Bush et al.[20] report that the bed porosity (ε_b) for full-scale coal-fired power plants employing a baghouse for particulate control ranges from 0.57 to 0.86.

RESULTS AND DISCUSSION

Table 1 lists baseline model parameters that were used in this study. It is important to note that these parameters were not arbitrarily chosen but that they reflect realistic conditions in powdered sorbent injection systems. For example, isotherm parameters listed in Table 1 correspond to the parameters that were obtained for the experimentally measured Hg removals at 275 °F as will be

Table 1. Base case scenario for the model.

Varied Parameters	
Parameter	**Value**
q_{max}	3020 μg/g
b	3.9 $m^3/\mu g$
C_o	5 $\mu g/m^3$
Q	1 m^3/sec
$\dot{m}_c$	0.025 g/sec
r_p	0.0015 cm
d_p	150 Å
τ_p	7.5
ε_b	0.7
ε_{cb}	0.005
Time in duct	2 sec

Fixed Parameters	
Parameter	**Value**
T	275 °F
ρ_p	2.04 g/cm^3
ε_p	0.67
A	50 m^2
Cleaning cycle interval	1500 sec
Fraction of filter cleaned per cycle	0.1

discussed in the second paper of this series. That paper also provides detailed discussion about other parameters listed in Table 1.

Figure 2 shows the predicted removal that can be accomplished in the duct for a 2-sec contact time as well as the removal of Hg from the section of the baghouse filter that is equal to one-tenth of the total filter area and overall Hg removal in the baghouse using the hypothetical base-case scenario shown in Table 1. The removal of Hg in the ductwork is limited by mass transfer from the bulk flue gas to the adsorbent particle and is relatively small (2.3%) for a 2-sec flight time. As the carbon particles are retained on the filter, the additional detention time allows the carbon particles to remove more Hg from the flue gas. This is shown by the increase in fractional removal with time from the section that is comprised of the one-tenth of the total filter area. Cleaning this section of the filter after 15,000 sec results in the complete removal of the accumulated adsorbent and subsequent reduction in the fractional removal to the levels equal to those at the exit from the ductwork. If one-tenth of the total filter area is cleaned every 1500 sec, then different sections of the filter are removing Hg at different levels depending on the depth of the accumulated adsorbent bed at that section. The overall Hg removal is thus a composite average of the removal in different sections of the fabric filter, and the profile of Hg removal will have a jagged nature because of the intermittent partial cleaning of the filter. The overall removal never decreases to the levels equal to those at the exit from the ductwork, and the average Hg removal efficiency under the base conditions shown in Table 1 is 87.5%.

Parameter Sensitivity

Because experiments can often be resource intensive, a model's ability to estimate the process performance caused by a change in an operating condition can be invaluable. Furthermore, it is also necessary to understand changes in the model predictions caused by uncertainties in the process variables. Thus, the sensitivity of the model predictions (i.e., the average Hg removal) as a function of various parameters is performed and is compared with the hypothetical base case shown in Table 1.

Isotherm Parameters. The impact of isotherm parameters on Hg removal efficiency from the baghouse is shown in Figure 3. Higher values of b (hence, higher forward rates of adsorption relative to desorption) resulted in higher removal efficiency. However, varying b more than 2 orders of magnitude only slightly impacted the removal efficiency relative to the base conditions. Increasing q_{max} by 1–2 orders of magnitude had a more significant impact on the removal efficiency. This would indicate that using carbons with higher adsorptive capacity could be beneficial assuming all other parameters and process conditions are similar. At high values of q_{max} and b the isotherm tends toward a constant isotherm and the fractional removal converges toward a constant value where the percent removal is governed by mass transfer.

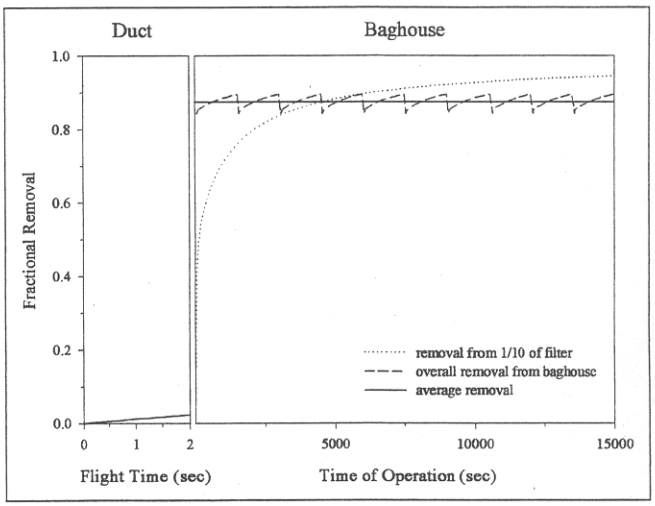

Figure 2. Dynamic profile of Hg removal from a 1/10 section of the baghouse filter and from the overall baghouse filter system.

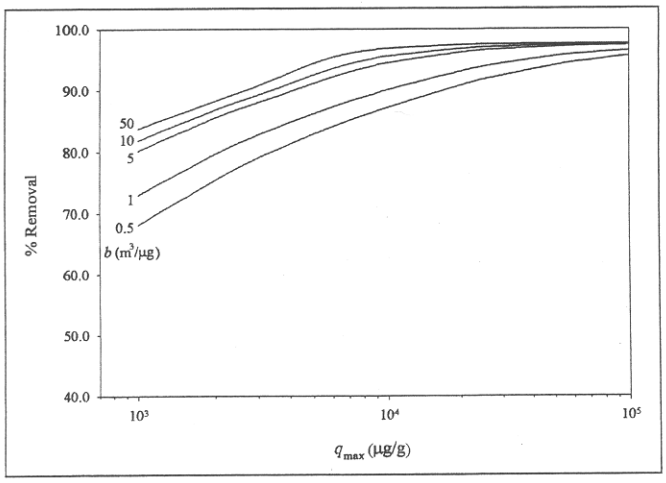

Figure 3. The effects of the isotherm parameters on the calculated average Hg removal efficiency from the baghouse filter.

Carbon Injection Rate and Flue Gas Parameters. Increasing the carbon injection rate (hence, increasing the C/Hg ratio) will increase the removal efficiency because more carbon capacity is available for Hg removal (Figure 4). The magnitude of the improvement in removal efficiency at higher C/Hg ratios decreases as Hg removal becomes more mass transfer-limited. Uncertainty in the carbon porosity of the bed does not significantly impact the calculated Hg removal efficiency.

Figure 5 shows the impact of the influent Hg concentration and the flow rate on the removal efficiency. Higher influent Hg concentrations result in lower C/Hg ratios and a lower removal efficiency. Higher gas flow rates result in higher velocities in the bed and higher mass transfer coefficients that should improve the removal efficiencies. However, for a fixed influent Hg concentration, a higher gas flow rate also results in a lower C/Hg ratio. Overall, higher gas flow rates result in lower removal efficiencies.

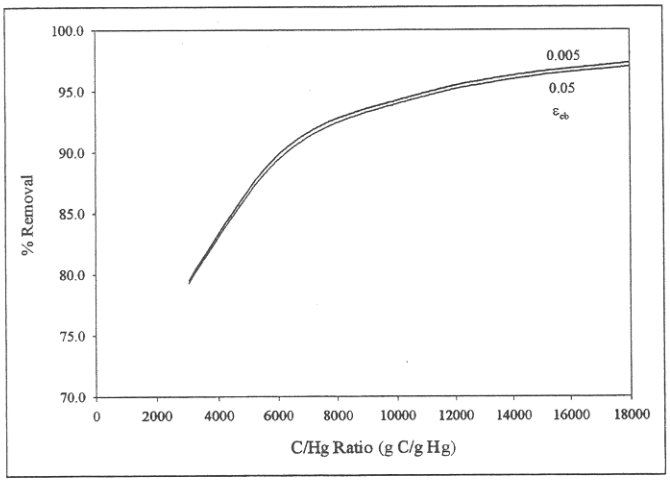

Figure 4. The effects of the carbon dose and the carbon porosity in the bed on the calculated average Hg removal efficiency from the baghouse filter.

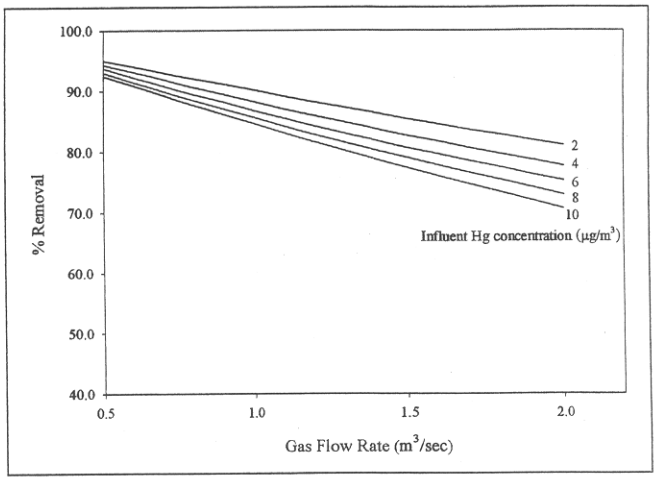

Figure 5. The effects of the influent Hg concentration and the gas flow rate on the calculated average Hg removal efficiency from the baghouse filter.

Sorbent Characteristics. The size of carbon particles injected upstream of the baghouse filter is another process parameter that can potentially be varied to control Hg removal efficiency. Under the base conditions and in the range of reasonable carbon particle radii, using smaller carbon particles will enhance the rate of Hg mass transfer from the bulk solution to the particle and result in better Hg removal from the baghouse filter (Figure 6). Also shown in Figure 6 is the impact of the bed porosity on the predicted removal efficiency. The range of the bed porosities investigated in this study corresponds to the range reported by Bush et al.[20] for full-scale coal-fired power plants employing a baghouse for particulate control. Figure 6 also demonstrates that uncertainty in bed porosity will not significantly impact predicted Hg removal efficiency from the baghouse filter.

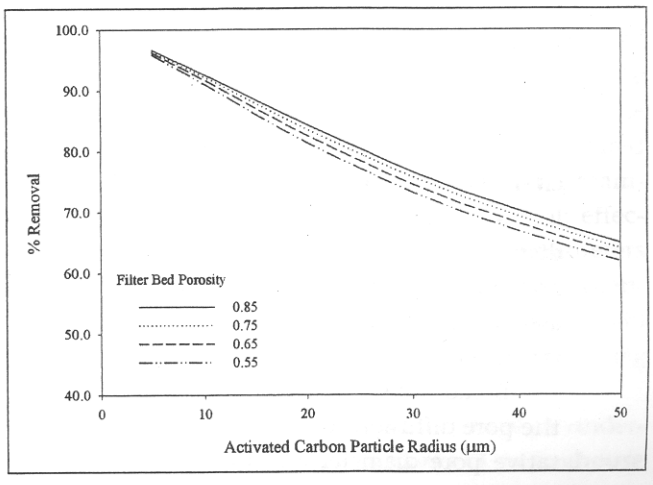

Figure 6. The effects of the activated carbon particle radius and the filter bed porosity on the calculated average Hg removal efficiency from the baghouse filter.

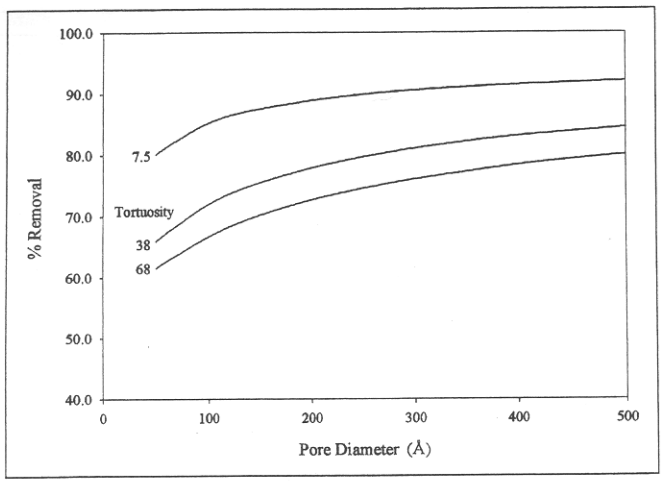

Figure 7. The effects of the pore diameter and tortuosity in the activated carbon particles on the calculated average Hg removal efficiency from the baghouse filter.

Figure 7 shows that the pore diameter and tortuosity significantly impacts the predicted Hg removal efficiency from the baghouse filter. These parameters are used in the calculation of the pore diffusion coefficient (eqs 52 and 53). An increase in the pore diameter increases the Knudsen diffusivity, which increases the pore diffusion coefficient. Larger pore diameters allow Hg to diffuse more freely into the pores, thereby increasing the intraparticle mass transfer rates and effectively removing more Hg from the bulk. In contrast, an increase in tortuosity means that Hg molecules must travel a longer distance as they diffuse from the activated carbon surface into the particle. The resulting decrease in the pore diffusion coefficient decreases the intraparticle mass transfer rate and reduces Hg removal efficiency.

Although activated carbon pore size distribution measurements are performed routinely, the choice of the representative pore diameter that adequately describes the distribution is still an unresolved issue that requires further research. In contrast, pore tortuosity cannot be measured directly. One approach is to perform kinetic experiments to evaluate the pore diffusion coefficient, characterize the pore size distribution of the particle, select a representative pore diameter from the pore size distribution, and back-calculate the tortuosity from eqs 52 and 53. This approach will still suffer from problems associated with the selection of an appropriate representative pore size diameter.

Because the main parameter required for the model is the pore diffusion coefficient, the selection of a representative pore diameter and tortuosity can be avoided by obtaining the coefficient directly from kinetic experiments at various temperatures. It is critical that the pore diffusion coefficient be estimated from the appropriate experimental data. Well-controlled and well-characterized kinetic experiments (e.g., fixed-bed experiments) that provide time-dependent Hg measurements can be used to estimate the pore diffusion coefficient as well as adsorption capacities at various temperatures.

Residence Time in the Duct. Figure 8 shows the impact of the residence time in the duct on the removal efficiency from both components of the system. An increase in the flight time enhances the removal efficiency in the duct because the adsorption of Hg by activated carbon is mass transfer-limited. The relationship between the flight time and duct removal efficiency is highly linear, indicating that the external mass transfer resistance limits the removal. From an overall process standpoint, the flight time in the duct appears to be irrelevant, because it does not significantly impact the overall removal efficiency from the baghouse as predicted by this model.

Evaluation of Scala's Model

Scala[7,8] was among the first to address the moving boundary problem associated with a growing adsorbent layer on a filter bed. However, there are several concerns with Scala's model as described in the literature. First, it is not clear if the model's governing equations are correct because the model does not account for the simultaneous presence of different solid phases (i.e., activated carbon and fly ash) in the baghouse filter. The model shows that the volume of the adsorbent in the bed (i.e., either activated carbon or fly ash) is equal to one minus the porosity of the bed, thus neglecting the other solid phase. Second, the effect of dispersion, which impacts the flux of Hg out of the filter bed, is neglected. Third, the accuracy of the model solution procedure with respect to numerical mass balance errors is not indicated. This accuracy is critical in

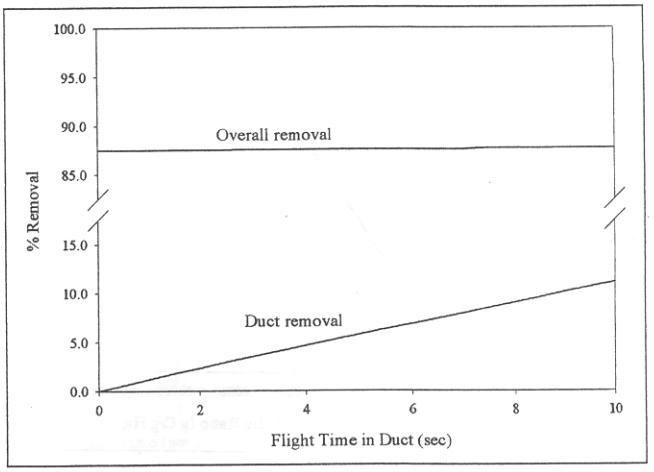

Figure 8. The effects of the flight time in the duct on the calculated Hg removal efficiency from the duct and the baghouse filter.

any modeling endeavor, and simply reporting the accuracy of the integration subroutine is not sufficient. The model solution procedure outlined in this study produces numerical mass balance errors that are consistently below 10^{-8}%. Furthermore, the coordinate transformation method used to solve the current model is more elegant and numerically superior to the upwind finite difference scheme used by Scala because it makes the model more amenable to numerical solution using conventional numerical procedures.[21,22]

One primary difference between Scala's model and the current work is that equilibrium was not assumed and kinetic resistance was accounted for on top of the diffusional resistance. To obtain an identical model to Scala, the following equations were substituted in the current model:

$$\frac{dq_p}{dt} = k_{for}(q_{max} - q_p)c_p - k_{rev}q_p \qquad (5a)$$

$$\frac{dQ_p}{dt} = \lambda_5[(1 + bc_o - bc_oQ_p)C_p - Q_p] \qquad (16a)$$

$$\frac{\partial Q_p}{\partial \tau} - \frac{\eta B_g}{x_0 + B_g\tau}\frac{\partial Q_p}{\partial \eta} = \lambda_6[(1 + bc_o - bc_oQ_p)C_p - Q_p] \qquad (51a)$$

Because the model solution procedure used by Scala is different, direct comparison of the calculations of the current model (with revised eqs 5a, 16a, and 51a) with Scala's model is impossible without having Scala's program. A comparison also requires that identical input files be used. Thus, only the premises of Scala's model can be evaluated. Although this approach inherently assumes that the current model and Scala's model will produce the same results if the premises are the same, this assumption is not necessarily true because of the differences in solution procedure. These premises are tested using the base case shown in Table 1 and assuming values for k_{rev} ranging from 10^{-4} to 10^{-2} sec^{-1}, which was within the range reported by Karatza et al.[23] Note that $b = k_{for}/k_{rev}$.

The first premise is that the volume of the adsorbent in the bed (i.e., activated carbon) is equal to one minus the porosity of the bed. This is tested by setting $\varepsilon_{cb} = 1 - \varepsilon_b$ in the current model, resulting in a difference of less than 0.5% between model calculations. This difference is negligible, which is consistent with the observations in Figure 4. However, this premise would also result in an unrealistic calculated final thickness of the bed before cleaning of 0.037 mm (vs. 2.2 mm for the current model). Bush et al.[20] reported a cake thickness ranging from 0.86 to 8.7 mm for full-scale coal-fired power plants employing a baghouse for particulate control.

The second premise is that the dispersion in the bed is negligible. The Peclet number for the base case in this study is calculated to be 0.09, which means that the dispersion is important. As expected, when the Peclet number is set at a very high value (10^8) to eliminate the impact of dispersion, the model calculates 5.8–8.9% higher removal efficiencies for the range of k_{rev} from 10^{-2} to 10^{-4} sec^{-1}, respectively. Neglecting dispersion produces a smaller flux of Hg out of the bed and allows more time for the activated carbon to adsorb Hg from the bulk gas phase. Although the relative difference may seem small considering the uncertainties generally associated with Hg control models, it does indicate a large absolute difference. This is critical, particularly because Scala specifically indicated that the difference in the model output variables resulting from neglecting axial dispersion was less than 1%. Hence, it is possible that the numerical solution procedure used by Scala may not be entirely accurate.

CONCLUSIONS

Mercury removal in the activated carbon particle was modeled using a pore diffusion model with the Langmuir isotherm describing equilibrium between the gas phase and the carbon particle surface. Mercury removal in the duct was modeled using a plug flow system, while mercury removal in the fabric filter was modeled using a growing-bed packed-bed approach. The presence of an external mass transfer boundary layer was accounted for in both stages. Advection, dispersion, and periodic cleaning were accounted for in the model of a growing packed bed on the fabric filter. Coordinate transformation was used to fix the spatial coordinates of the growing bed, making the model amenable to solving using orthogonal collocation techniques.

In any modeling study, adequate estimation of the model parameters is needed for accurate predictions. The key parameters that significantly impact the calculated average removal include the adsorption isotherm parameters and the carbon pore radius and tortuosity (or effectively, the pore diffusion coefficient). These parameters can be obtained from properly designed kinetic experiments. Critical baghouse operational parameters that will determine the calculated Hg removal include the C/Hg ratio and the carbon particle size.

An avenue of further work that is critical to understanding and predicting the performance of the baghouse filter is an investigation of the role of increasing pressure drop in the system. In this study, the flow rate across the baghouse filter and cake is assumed to be constant with

time. In reality, the pressure buildup across the filter cake decreases the flow rate, which would increase the removal efficiency because of the additional contact time available for Hg adsorption from the bulk solution. However, as a fraction of the filter bed is cleaned, the higher flow rate associated with the lower pressure drop across this particular section of the filter will result in a lower removal efficiency. Further work is necessary to understand the role of the pressure drop in the dynamics of Hg removal from the baghouse filter system.

ACKNOWLEDGMENTS

This work was funded in part by the National Energy Technology Laboratory of the U.S. Department of Energy under Contract No. DE-AM26-99FT40463, Subtask No. FT10241. The findings and conclusions expressed in this manuscript are solely of the authors and do not necessarily reflect the views of the funding agency. Reference in this manuscript to any specific commercial product, process, or service is to facilitate understanding and does not necessarily imply its endorsement or favoring by the U.S. Department of Energy. The authors also acknowledge Dr. Byung Kim from Ford Motor Company for valuable discussions on the numerical methods used in this study.

NOMENCLATURE

A = surface area of the baghouse filter (m^2)
b = Langmuir isotherm coefficient ($m^3/\mu g$)
B_g = dimensionless bed growth (−)
Bi_d = Biot number in the duct (−)
Bi_f = Biot number in the baghouse filter (−)
C_{ave} = average concentration in the particle normalized to c_o (−)
c_{ave} = average concentration in the particle ($\mu g/m^3$)
C_b = concentration in the bulk normalized to c_o (−)
c_b = concentration in the bulk ($\mu g/m^3$)
c_o = influent concentration ($\mu g/m^3$)
C_p = concentration in the particle normalized to c_o (−)
c_p = concentration in the particle ($\mu g/m^3$)
C/Hg = carbon to mercury ratio (g/g)
D = dispersion coefficient (cm^2/sec)
D_{Hg} = diffusion coefficient of Hg in air (cm^2/sec)
D_{Kn} = Knudsen diffusion coefficient (cm^2/sec)
D_p = pore diffusion coefficient (cm^2/sec)
d_{pore} = pore diameter (Å)
D_s = surface diffusion coefficient (cm^2/sec)
E = composite porosity, see eq 36 (−)
k_f = film mass transfer coefficient (cm/sec)
k_{for} = forward rate of adsorption ($m^3/\mu g$-sec)
k_{rev} = reverse rate of adsorption (i.e., desorption rate) (1/sec)
L = depth of the baghouse filter bed (cm)
L_{max} = maximum depth of the baghouse filter bed before cleaning (cm)
L_0 = initial depth of the baghouse filter bed = $10^{-7}L_{max}$ (cm)
$\dot{m}_c$ = activated carbon injection rate (g/sec)
MW_{Hg} = molecular weight of mercury (g/mol)
Pe = Peclet number (−)
Q = gas flow rate (m^3/sec)
Q_{ave} = average mass of adsorbate per mass of adsorbent normalized to q_o (−)
q_{ave} = average mass of adsorbate per mass of adsorbent ($\mu g/g$)
q_{max} = maximum mass of adsorbate per mass of adsorbent ($\mu g/g$)
q_o = mass of adsorbate per mass of adsorbent in equilibrium with c_o ($\mu g/g$)
Q_p = mass of adsorbate per mass of adsorbent normalized to q_o (−)
q_p = mass of adsorbate per mass of adsorbent ($\mu g/g$)
R = dimensionless radial distance (−)
r = radial distance (cm)
r_p = particle radius (cm)
T = temperature (°F)
t = time (sec)
T_d = dimensionless time in the duct (−)
T_f = dimensionless time in the baghouse filter (−)
T_k = absolute temperature (K)
$v = Q/A\varepsilon_b$ = interstitial velocity (cm/sec)
v_o = relative velocity between adsorbent particles and flue gas stream (cm/sec)
X = dimensionless axial distance (−)
x = axial distance (cm)
X_0 = dimensionless initial bed depth of the baghouse filter (−)

Greek Symbols

ε_b = bed porosity (cm^3 bed pores/cm^3 total bed volume)
ε_{cb} = carbon porosity in the bed (cm^3 total AC volume/cm^3 total bed volume)
ε_p = internal porosity of adsorbent (cm^3 AC pores/cm^3 total AC volume)
η = dimensionless axial distance (−)
λ_1 = dimensionless parameter, see eq 10 (−)
λ_2 = dimensionless parameter, see eq 10 (−)
λ_3 = dimensionless parameter, see eq 10 (−)
λ_4 = dimensionless parameter, see eq 36 (−)
λ_5 = dimensionless parameter = $k_{rev}k_p^2/D_p$, see eq 51a (−)

λ_6 = dimensionless parameter = $k_{rev}L_{max}/v$, see eq 51a (−)

ν = kinematic viscosity of air (cm^2/sec)

ρ_p = material density of adsorbent (g/cm^3 AC material)

τ = dimensionless time (−)

τ_p = tortuosity in the pore (−)

ξ = dimensionless radial distance (−)

REFERENCES

1. Chen, S.; Rostam-Abadi, M.; Chang, R. *Proceedings of the 211th ACS National Meeting,* New Orleans, LA, March 24–28, 1996; Vol 41, pp 442–446.
2. Rostam-Abadi, M.; Chen, S.G.; Hsi, H.-C.; Rood, M.; Chang, R.; Carey, T.; Hargrove, B.; Richardson, C.; Rosenhoover, W.; Meserole, F. *Proceedings of the First EPRI-DOE-EPA Combined Utility Air Pollution Control Symposium,* Session B; Washington DC, Aug 25–29, 1997.
3. Flora, J.R.V.; Vidic, R.D.; Liu, W.; Thurmau, R.C. *J. Air & Waste Manage. Assoc.* **1998**, *48*, 1051–1059.
4. Meserole, F.B.; Chang, R.; Carrey, T.R.; Machac, J.; Richardson, C.F. *J. Air & Waste Manage. Assoc.* **1999**, *49*, 694–704.
5. Serre, S.D.; Gullett, B.K.; Ghorishi, S.B. *J. Air & Waste Manage. Assoc.* **2001**, *51*, 733–741.
6. Serre, S.D.; Silcox, G.D. *Ind. Eng. Chem. Res.* **2000**, *39*, 1723–1730.
7. Scala, F. *Environ. Sci. Technol.* **2001**, *35*, 4367–4372.
8. Scala, F. *Environ. Sci. Technol.* **2001**, *35*, 4373–4378.
9. Manes, M. Activated Carbon Adsorption Fundamentals. In *Encyclopedia of Environmental Analysis and Remediation;* Meyers, R.A., Ed.; Wiley and Sons: New York, 1998.
10. Finlayson, B.A. *Nonlinear Analysis in Chemical Engineering;* McGraw-Hill: New York, 1980.
11. Brenan, K.E.; Campbell, S.L.; Petzold, L.R. *Numerical Solution of Initial-Value Problems in Differential-Algebraic Equations;* North-Holland: New York, 1989.
12. Crank, J. *Free and Moving Boundary Problems;* Oxford University Press: New York, 1984.
13. Knudsen, J.G.; Hottel, H.C.; Sarofim, A.F.; Wankat, P.C.; Knaebel, K.S. Section 5—Heat and Mass Transfer. In *Perry's Chemical Engineer's Handbook,* 7th ed.; Green, D.W., Maloney, J.O., Eds.; McGraw-Hill: New York, 1997.
14. Cussler, E.L. *Diffusion: Mass Transfer in Fluid Systems;* Cambridge University Press: New York, 1984.
15. Ruthven, D.M. *Principles of Adsorption and Adsorption Processes;* Wiley and Sons: New York, 1984.
16. Wark, K.; Warner, C.F. *Air Pollution: Its Origin and Control;* Harper and Row: New York, 1981.
17. Wakao, N.; Funazkri, T. *Chem. Eng. Sci.* **1978**, *33*, 1375–1384.
18. Hsi, H.-C.; Chen, S.; Rostam-Abadi, M.; Rood, M.J.; Richardson, C.F.; Carey, T.R.; Chang, R.L. *Energy Fuels* **1998**, *12*, 1061–1070.
19. Yang, R.T. *Gas Separation by Adsorption Processes;* Butterworth's Inc.: Boston, 1987.
20. Bush, P.V.; Snyder, T.R.; Chang, R.L. *J. Air Pollut. Control Assoc.* **1989**, **39**(2), 228–237.
21. Furzeland, R.M. *J. Inst. Math. Appl.* **1980**, *26*, 411–429.
22. Kutluay, S.; Bahadir, A.R.; Ozdes, A. *J. Comput. Appl. Math.* **1997**, *81*, 135–144.
23. Karatza, D.; Lancia, A.; Musmarra, D; Pepe, F.; Volpicelli, G. *Haz. Waste & Haz. Materials,* **1996**, *13*, 95-105.

About the Authors

Joseph R.V. Flora is an associate professor in the Department of Civil and Environmental Engineering, University of South Carolina, Columbia, SC 29208. Richard A. Hargis, William J. O'Dowd, and Henry W. Pennline are chemical engineers in the National Energy Technology Laboratory, U.S. Department of Energy, P.O. Box 10940, Pittsburgh, PA 15236. Radisav D. Vidic is an associate professor in the Department of Civil and Environmental Engineering, University of Pittsburgh, Pittsburgh, PA 15261.